J. Fluid Mech. (1978), *vol.* 87, *part* 2, *pp.* 305–319
Printed in Great Britain

Two-dimensional turbulence on the surface of a sphere

By CHA-MEI TANG† AND STEVEN A. ORSZAG
Department of Mathematics, Massachusetts Institute of Technology, Cambridge

(Received 25 August 1977)

Large-scale atmospheric flow shares certain attributes with two-dimensional turbulence. In this paper, we study the effect of spherical geometry on two-dimensional turbulence.

Energy transfer is multi-component in spherical geometry in contrast to energy transfer among triads of wave vectors in Cartesian geometry. It follows that energy transfer is more local in spherical than in Cartesian geometry. Enstrophy transfer to higher wavenumbers in spherical geometry is less than enstrophy transfer to higher wavenumbers in Cartesian geometry. Since both energy and enstrophy are inviscid constants of motion, the back transfer of energy is also less in spherical than in Cartesian geometry. Therefore, with a finite viscosity, enstrophy decays more slowly in spherical geometry than in Cartesian geometry. Here these conjectures are tested numerically by spectral methods. The numerical results agree well with the conjectures.

1. Introduction

In this paper, we compare two-dimensional turbulent flows on the surface of a sphere with two-dimensional turbulent flows in Cartesian geometry. Two-dimensional turbulent flow in Cartesian geometry has been the subject of much study (Onsager 1949; Lee 1951; Fjørtoft 1953; Kraichnan 1967; Batchelor 1969; Lilly 1971; Leith 1971; Herring *et al.* 1974). While two-dimensional turbulence is not yet realizable in the laboratory, it is thought that these flows are relevant to atmospheric dynamics. Three-dimensional quasi-geostrophic flow in the atmosphere away from the equator was found by Charney (1971) to exhibit two scalar invariants, the total kinetic energy and mean-square 'pseudo-potential vorticity', similar to the quadratic invariants of inviscid two-dimensional turbulence.

In §2, we review the important concepts of two-dimensional turbulence in Cartesian geometry. In §3, we formulate the problem in spherical geometry. We shall show that the appropriate two-dimensional wavenumber for flows on the sphere is the degree n, not the order m of the surface harmonic Y_n^m. Energy and enstrophy transfer will be shown to be more local in wave space for two-dimensional turbulence on a sphere than for planar turbulence. The consequences of this locality of transfer on spheres will be discussed and substantiated by numerical results in §4.

† Present address: Applied Physics Laboratory, The Johns Hopkins University, Laurel, Maryland.

2. Two-dimensional turbulence in Cartesian co-ordinates

In two-dimensional, inviscid, incompressible flow, vortex tubes move with the fluid. Vortex tubes cannot be stretched, so enstrophy (mean-square vorticity) cannot be produced. Therefore, for two-dimensional, homogeneous, isotropic turbulence, kinetic energy and also enstrophy are inviscid constants of motion. These inviscid constraints have a profound effect on the nature of viscous turbulence. Unlike the predominantly one-way transfer of energy to the small scales in three-dimensional turbulence, energy is transferred to the large scales and enstrophy is transferred to the small scales in two dimensions.

The concepts of two-dimensional turbulence in Cartesian geometry may be illustrated by a flow confined within a cyclic box with sides of length 2π. The vorticity $\zeta\hat{\mathbf{i}}_z$ is defined as $\nabla \times \mathbf{u}$, where $\mathbf{u}$ is the velocity. In two dimensions, $\mathbf{u}$ can be represented in terms of a stream function ψ as $-(\nabla\psi) \times \hat{\mathbf{i}}_z$. Here ζ, ψ and $\mathbf{u}$ are functions of (x, y, t). In terms of the vorticity and stream function, the Navier–Stokes equations are

$$\partial\zeta/\partial t = -J(\psi, \zeta) + \nu\nabla^2\zeta, \tag{1}$$

where $J(\psi, \zeta) = \partial(\psi, \zeta)/\partial(x, y)$ and ν is the kinematic viscosity, and

$$\zeta = \nabla^2\psi. \tag{2}$$

When ζ and ψ are expanded in the Fourier series

$$\zeta = \sum_{\mathbf{k}} \zeta(\mathbf{k})\, e^{i\mathbf{k}\cdot\mathbf{x}}, \quad \psi = \sum_{\mathbf{k}} \psi(\mathbf{k})\, e^{i\mathbf{k}\cdot\mathbf{x}}, \tag{3}$$

reality of $\zeta(\mathbf{x})$ and $\psi(\mathbf{x})$ requires that $\zeta(\mathbf{k}) = \zeta^*(-\mathbf{k})$ and $\psi(\mathbf{k}) = \psi^*(-\mathbf{k})$. In a numerical simulation of (1) and (2) by spectral methods only a finite number of modes are retained in (3) (Herring *et al.* 1974).

The energy in mode $\mathbf{k}$ is

$$U(\mathbf{k}) = (8\pi^2)^{-1} \int |\nabla\psi|^2\, d\mathbf{x} = \tfrac{1}{2}k^2|\psi(\mathbf{k})|^2, \tag{4}$$

where $k = |\mathbf{k}|$. The energy balance equation is

$$(\partial/\partial t + 2\nu k^2)\, E(k) = T(k), \tag{5}$$

where

$$T(k) = \sum_{|\mathbf{k}|=k} \sum_{\mathbf{p}+\mathbf{q}=\mathbf{k}} T(\mathbf{k}, \mathbf{p}, \mathbf{q})$$

and

$$E(k) = \sum_{|\mathbf{k}|=k} U(\mathbf{k})$$

is the energy in the wavenumber k. $T(\mathbf{k}, \mathbf{p}, \mathbf{q})$ is the energy in mode $\mathbf{k}$ gained from wavenumbers $\mathbf{p}$ and $\mathbf{q}$: explicitly,

$$T(\mathbf{k}, \mathbf{p}, \mathbf{q}) = \begin{cases} |\mathbf{q} \times \mathbf{p}|\, [\zeta(\mathbf{p})\psi(\mathbf{q})\psi(-\mathbf{k}) - \psi(\mathbf{p})\zeta(\mathbf{q})\psi(-\mathbf{k})] & \text{for} \quad \mathbf{k} = \mathbf{p}+\mathbf{q}, \\ 0 \quad \text{otherwise.} \end{cases} \tag{6}$$

The enstrophy of mode $\mathbf{k}$ is

$$(8\pi^2)^{-1} \int \zeta^2\, d\mathbf{x} = \tfrac{1}{2}\,|\zeta(\mathbf{k})|^2 = k^2 U(\mathbf{k}). \tag{7}$$

The total energy and enstrophy are related by

$$dE/dt = -2\nu F, \quad dF/dt = -\eta, \tag{8}$$

where $$E = \sum_{\mathbf{k}} E(k), \quad F = \sum_{\mathbf{k}} k^2 E(k), \quad \eta = 2\nu \sum_{\mathbf{k}} k^4 E(k)$$

are the total energy, enstrophy and enstrophy dissipation rate respectively.

In Cartesian geometry, energy conservation involves only triads of modes and is expressed by the relation

$$T(\mathbf{k}, \mathbf{p}, \mathbf{q}) + T(\mathbf{p}, \mathbf{q}, \mathbf{k}) + T(\mathbf{q}, \mathbf{k}, \mathbf{p}) = 0 \tag{9}$$

for $\mathbf{k} = \mathbf{p} + \mathbf{q}$. Conservation of enstrophy is expressed by the triad relation

$$k^2 T(\mathbf{k}, \mathbf{p}, \mathbf{q}) + p^2 T(\mathbf{p}, \mathbf{q}, \mathbf{k}) + q^2 T(\mathbf{q}, \mathbf{k}, \mathbf{p}) = 0. \tag{10}$$

If one of the modes $\mathbf{k}$, $\mathbf{p}$ or $\mathbf{q}$ is the source or sink for energy and enstrophy transfer, it must be the intermediate wavenumber.

Kraichnan (1967) showed that the existence of the two inviscid constants of motion, energy and enstrophy, implies that two-dimensional turbulence admits two formal inertial ranges. If turbulence is forced isotropically at a wavenumber $k \sim k_i$, then a $k^{-\frac{5}{3}}$ backwards-energy-transfer inertial range should be found for $k \ll k_i$ and a k^{-3} enstrophy-transfer inertial range should be found for $k \gg k_i$.

Several scales of wavenumbers and Reynolds numbers have been introduced to characterize two-dimensional turbulence. Following Lilly (1971) and Herring *et al.* (1974) the large-scale Reynolds number R_L is defined as

$$R_L = E\nu^{-1}\eta^{-\frac{1}{3}}. \tag{11}$$

The enstrophy-dissipation wavenumber is defined as

$$k_\eta = \eta^{\frac{1}{6}}\nu^{-\frac{1}{2}}. \tag{12}$$

The quantitative theory of the enstrophy-transfer inertial range suggests that $k^4E(k)$ decays rapidly for $k \gg k_\eta$ and that wavenumbers much larger than k_η have no significant effect on wavenumbers smaller than k_η. In other words, the scales that contribute to the energy and enstrophy dynamics are $k \lesssim k_\eta$.

A non-dimensional measure of the rate of production of the mean-square vorticity gradient is the two-dimensional skewness factor

$$S_2 = [\sum_{\mathbf{k}} k^4 T(k)]\, 2\nu\eta^{-1}F^{-\frac{1}{2}}. \tag{13}$$

3. Two-dimensional turbulence on a sphere

For flow on the surface of a unit sphere, only the θ and ϕ components of the velocity $\mathbf{u}$ are non-zero. Therefore the vorticity is given by $\zeta\hat{\mathbf{i}}_r = \nabla \times \mathbf{u}$ and the velocity can be represented by a Stokes stream function as $\mathbf{u} = -(\nabla\psi) \times \hat{\mathbf{i}}_r$. The equations of motion in a rotating co-ordinate system are

$$\partial\zeta/\partial t = J(\psi, \zeta) + \nu\nabla^2\zeta - 2\Omega\partial\psi/\partial\phi, \tag{14}$$

where $$J(\psi, \zeta) = \partial(\psi, \zeta)/\partial(\cos\theta, \phi),$$

and $$\zeta = \nabla^2\psi. \tag{15}$$

Here Ω is the angular velocity of the sphere.

Since ζ and ψ are scalar variables, they may be expanded as

$$(\psi, \zeta) = \sum_{|m|=0}^{N} \sum_{n=|m|}^{N} (\psi_{nm}, \zeta_{nm})\, Y_n^m(\theta, \phi). \tag{16}$$

Here $Y_n^m(\theta, \phi)$, the surface harmonic of degree n and order m, is defined as

$$Y_n^m(\theta, \phi) = b_{nm} P_n^m(\cos\theta)\, e^{im\phi} \tag{17}$$

in terms of the associated Legendre polynomial $P_n^m(\cos\theta)$ and

$$b_{nm} = [(2n+1)(n-m)!]^{\frac{1}{2}}[4\pi(n+m)!]^{\frac{1}{2}}.$$

The velocity components u_θ and u_ϕ behave like vectors under a change of co-ordinate frame so they may be expanded as

$$(u_\theta, u_\phi) = \frac{1}{\sin\theta} \sum_{|m|=0}^{N} \sum_{n=|m|}^{N} (u_{nm}, v_{nm})\, Y_n^m(\theta, \phi). \tag{18}$$

There has been much work (Horn & Bryson 1963; Wiin–Nielsen 1967; Julian *et al.* 1970) on the analysis of the spectrum of large-scale kinetic energy in the atmosphere using the hemispherical wavenumber m. However, the one-dimensional wavenumber m cannot be used in the same way as the two-dimensional wavenumber k in Cartesian geometry. When large-scale motions of the atmosphere are of interest, curvature becomes significant and energy spectra should be expressed in terms of n. To see why, we recall that the physical significance of k^2 in Cartesian geometry is due to the fact that dissipation is proportional to $k^2E(k)$. In spherical geometry, dissipation of a mode of unit amplitude is proportional to $\nabla^2 Y_n^m = -n(n+1)\, Y_n^m$, which indicates that the most appropriate choice of wavenumber is n, not m. With n as the wavenumber, we obtain

$$E = \sum_{n=1}^{N} E(n), \tag{19}$$

where

$$E(n) = \tfrac{1}{2} \sum_{|m|=0}^{N} n(n+1)\, |\psi_{nm}|^2,$$

and

$$F = \sum_{n=1}^{N} n(n+1)\, E(n). \tag{20}$$

Baer (1972) was the first to propose the use of n as the wavenumber, and compared results analysed using n with those analysed using m. His expressions for $E(n)$ can be taken as only a rough approximation of the correct spectrum when the truncation N is large because he did not use (18) for the velocity expansion. Baer's results showed that the two different ways of analysing data lead to significant differences in the slopes of calculated spectra. The trend is that when the index n is used the peak of the energy $E(n)$ occurs at approximately $n = 8$–9. The behaviour of $E(n)$ for $n > 9$ is roughly given by $E(n) \propto n^{-3}$, at least for $9 \lesssim n \lesssim 30$. The same data analysed using m have a much steeper slope. Most of the energy lies in the lowest hemispherical wavenumbers. The region of the energy spectrum behaving like m^{-3} contains only about 10 wavenumbers.

Much data analysis from atmospheric observations involves only one component of the velocity, usually the east–west flow. The north–south flow is assumed to be in energy equipartition at high wavenumbers with the east–west flow. Special care is

required in this data analysis. Let us consider the single wave whose stream function is $\mathrm{Re}\,(\psi_{nm}\,Y_n^m)$. The corresponding velocity components are given by

$$u_{nm} = -im\psi_{nm} \tag{21a}$$

and

$$v_{n-1,m} = -(n+1)\,(n+m)\,(2n+1)^{-1}\psi_{nm}, \tag{21b}$$

$$v_{n+1,m} = n(n-m+1)\,(2n+1)^{-1}\psi_{nm}. \tag{21c}$$

The energy in the velocity in the θ direction is

$$\hat{E}_\theta(n,m) = \tfrac{1}{2}\int_0^{2\pi} d\phi \int_0^{\pi} |u_\theta|^2 \sin\theta\, d\theta = \tfrac{1}{2}(n+\tfrac{1}{2})\, m^{-1}|u_{nm}|^2. \tag{22a}$$

The energy in the velocity in the ϕ direction is

$$\hat{E}_\phi(n,m) = \frac{n-\frac{1}{2}}{2m}\,|v_{n-1,m}|^2 + \frac{n+\frac{3}{2}}{2m}\,|v_{n+1,m}|^2 + c\,\mathrm{Re}\,(v_{n-1,m}\,v^*_{n+1,m}), \tag{22b}$$

where

$$c = 2\pi b_{n-1,m}\,b_{n+1,m}\int_0^{\pi} \sin^{-1}\theta\, P^m_{n-1}(\theta)\, P^m_{n+1}(\theta)\, d\theta.$$

However, the use of u_{nm} and v_{nm} can be confusing. The total energy is $\frac{1}{2}n(n+1)\,|\psi_{nm}|^2$ and it belongs to the wavenumber n. The expressions for $\hat{E}_\theta(n,m)$ and $\hat{E}_\phi(n,m)$ are clearer when written in terms of the stream function ψ_{nm}:

$$\hat{E}_\theta = \tfrac{1}{2}(n+\tfrac{1}{2})\,m|\psi_{nm}|^2, \quad \hat{E}_\phi = \tfrac{1}{2}[n(n+1)-(n+\tfrac{1}{2})\,m]|\psi_{nm}|^2. \tag{23}$$

In isotropic turbulence, the average properties of ψ_{nm} are the same for all m for a given wavenumber n. Summing over all modes m gives

$$E_\theta(n) = \tfrac{1}{2}(n+\tfrac{1}{2})\sum_{m=0}^{n} m|\psi_{nm}|^2 \simeq \tfrac{1}{4}(n^3+\tfrac{1}{2}n^2)\,|\psi_{nm}|^2. \tag{24a}$$

Similarly,

$$E_\phi(n) \simeq \tfrac{1}{4}(n^3+\tfrac{3}{2}n^2)\,|\psi_{nm}|^2. \tag{24b}$$

When n is large, there is approximate partition of energy between the two components of kinetic energy.

Spectral analysis using m as the index is frequently preferred because it involves only Fourier transforms in ϕ. The calculation of $E(n)$ is more complicated. To effect this calculation, it is best to take advantage of the relationship between u_θ and ψ. u_{nm} can be calculated from $u_\theta(\theta,\phi)$ using Fourier transformation in ϕ and Gaussian quadrature in θ, while ψ_{nm}, which is needed to calculate the energy, is simply

$$\psi_{nm} = (imb_{nm})^{-1}u_{nm}.$$

If the flow is truly two-dimensional, u_ϕ is also uniquely determined by u_{nm}. The accuracy of the data analysis can be checked by comparing the u_ϕ computed from u_θ with data on u_ϕ.

The energy balance equation in spherical co-ordinates is

$$[\partial/\partial t + 2\nu n(n+1)]\,E(n) = T(n), \tag{25}$$

where $T(n)$ is the nonlinear energy transfer into modes n.

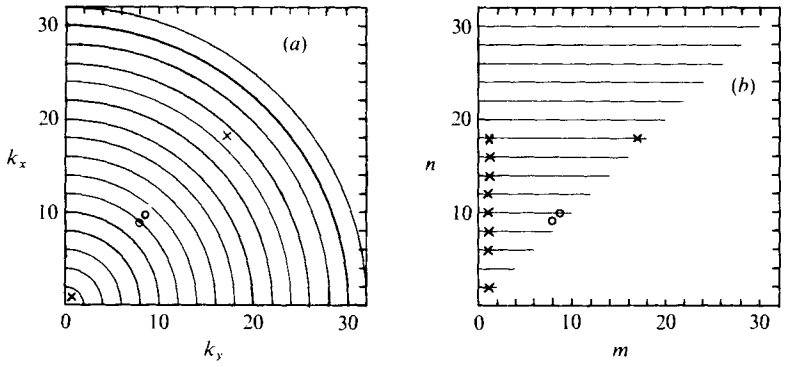

FIGURE 1. An example of nonlinear wave interaction in the two different geometries. (*a*) In Cartesian co-ordinates, the nonlinear transfer of two modes (9, 8) and (10, 9) results in energy and enstrophy changes for (1, 1) and (19, 17). (*b*) In spherical co-ordinates, the nonlinear transfer of two modes (9, 8) and (10, 9) results in energy and enstrophy changes for (2, 1), (4, 1) (which happens to be zero), (6, 1), (8, 1), (10, 1), (12, 1), (14, 1), (16, 1), (18, 1) and (18, 17).

Let us contrast the nature of nonlinear processes in Cartesian and spherical co-ordinates. In Cartesian geometry suppose that ψ is composed of two waves as follows:

$$\psi(x,y) = C_1[\cos(9x+8y)+\cos(10x+9y)], \tag{26a}$$

where the waves are denoted below as (9, 8) and (10, 9) and C_1 is a constant. The result of the nonlinear interaction $J(\psi, \zeta)$ consists of components (1, 1) and (19, 17). On the other hand, in spherical geometry the two-wave field

$$\psi(\theta,\phi) = C_2(P_9^8(\theta)\cos 8\phi + P_{10}^9(\theta)\cos 9\phi), \tag{26b}$$

where C_2 is another constant, results in the nonlinear terms (2,1), (4,1) (which is zero), (6,1), (8,1), (10,1), (12,1), (14,1), (16,1), (18,1) and (18,17). (See figure 1.) In, spherical co-ordinates the transfer in n is no longer limited to three wavenumbers. In figure 2(*a*) we have plotted the initial energy transfer functions in Cartesian and spherical geometries for this example. The enstrophy transfer functions in Cartesian and spherical geometries are plotted in figure 2(*b*).

The implications of the multi-component transfer mechanism in spherical geometry are significant. If a given amount of enstrophy leaving a wavenumber n is spread into more than two waves between p and q, the total energy transferred will also be spread between p and q. As a result, less energy will go to the lower wavenumbers in the multi-component spherical interaction than in the Cartesian triad interaction. The transfer of enstrophy to the larger scales will also be less in spherical geometry. Kraichnan (1967) assumed that nonlinear interaction is local in wavenumber space, so that significant interactions giving energy or enstrophy transfer take place only between comparable wavenumbers. This assumption is satisfied better in spherical geometry than in Cartesian geometry.

The definitions of the Reynolds number, the Kolmogorov dissipation wavenumber and the skewness factor in spherical geometry are given in (11)–(13), respectively, with E, F and η evaluated in terms of the spherical energy function $E(n)$ rather than the Cartesian function $E(k)$.

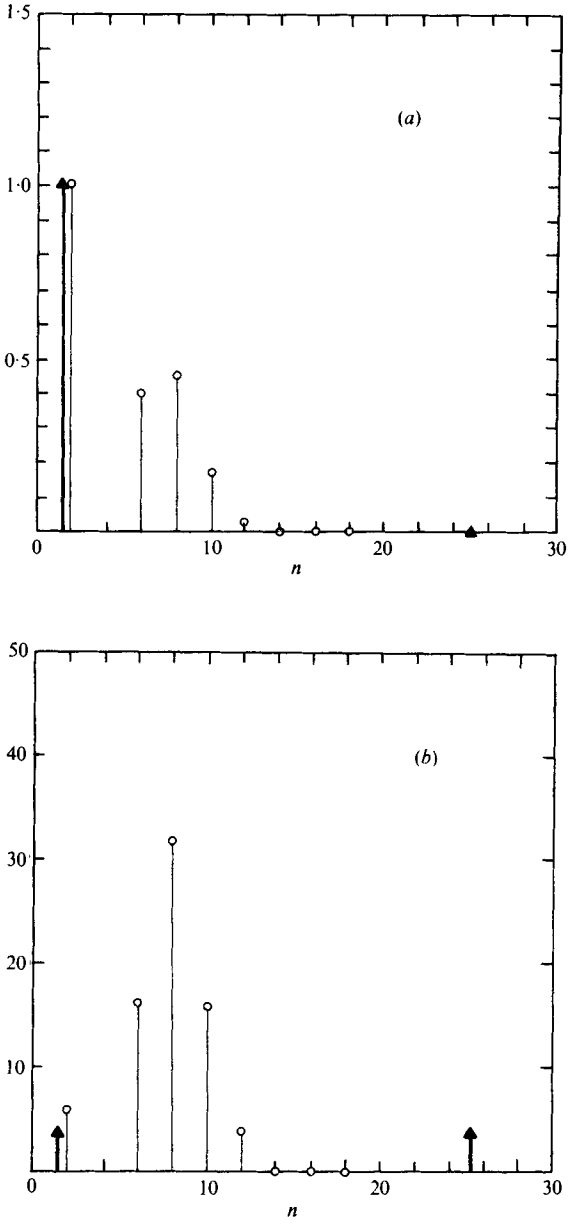

FIGURE 2. A plot of the initial rate of (*a*) energy and (*b*) enstrophy transfer to modes n in Cartesian and spherical geometry with an initial stream function given by (26). ▲, Cartesian geometry, stream function (26*a*) with C_1 chosen such that mode (1, 1) has unit amplitude; ○, spherical geometry, stream function (26*b*) with C_2 is chosen such that mode (2, 1) has unit amplitude.

4. Numerical results

We have used numerical simulation to verify some of the postulates in §3. The present calculations are analogous to those performed in a cyclic box in Cartesian geometry by Herring *et al.* (1974) using Fourier series and the pseudo-spectral method. The numerical methods used to solve (14) and (15) in spherical geometry are described elsewhere (Orszag 1974; Tang 1978).

In Cartesian geometry, Herring *et al.* generated an initial random field with an energy spectrum

$$E(k, t = 0) = u_0^2 \, (k/k_0) \exp(-k/k_0), \tag{27}$$

where $u_0 = 1$ and $k_0 = \frac{3}{2}$. They found that a good measure of the accuracy of simulation is that all scales of motion that make appreciable contributions to the enstrophy dissipation rate should be resolved. We know that $k^4 E(k)$ should decay exponentially for $k > k_\eta$. Thus Herring *et al.* found that spectral methods using a wavenumber truncation of 32 (64×64 modes) are marginally accurate for $\nu = 0{\cdot}0025$, or a Reynolds number of 350.

Let us now compare turbulence in Cartesian and spherical geometry. In spherical geometry, the initial energy spectrum is assumed to be (27) with k replaced by n. It is not possible to pick the initial conditions to be identical for spherical and Cartesian geometries. Only the energy spectra of the initial flows can be chosen equal.

Truncation at a wavenumber of 32 is used for all the simulations discussed below. Six calculations are compared: Cartesian geometry with $\nu = 0{\cdot}0025$ and $\nu = 0{\cdot}005$, spherical geometry with and without rotation and with $\nu = 0{\cdot}0025$ and $\nu = 0{\cdot}005$. The choices $\nu = 0{\cdot}005$ and $\nu = 0{\cdot}0025$ correspond to initial Reynolds numbers of 140 and 350, respectively. The results are plotted in figures 3–8. We make no attempt in this paper to investigate inertial-range spectra of turbulence on spheres because of the limited wavenumber cut-off at 32. It seems that effective investigation of the inertial range requires as least twice this resolution (see Herring *et al.* 1974).

As in Cartesian geometry, the enstrophy dissipation spectra plotted in figure 3 show that the highest initial Reynolds number that can be simulated accurately with truncation at a wavenumber of 32 is approximately 350. Further discussion of the accuracy of these calculations is given by Tang (1978). All the calculations reported here are believed to be in error by no more than 1 %.

For a given n, the energy is distributed evenly among all m modes in spherical geometry. This ensures that the initial conditions are isotropic. In this case, the turbulence should remain approximately isotropic at later times. In figure 4 we plot contours of $-\ln(E(n, m))$ at $t = 2{\cdot}88$. The lines of constant energy have remained approximately horizontal.

The two-dimensional skewness factor S_2 is a non-dimensional measure of the rate of production of enstrophy dissipation by the nonlinearity and is also an indication of the development of turbulence. In figure 5 we plot $S_2(t)$ *vs.* t for all six runs. In general, $S_2(t)$ grows rapidly for $t < 0{\cdot}5$ then levels off to a relatively steady value at later times. The turbulence is well established after $t = 1$; here we report results up to $t = 3{\cdot}0$. At the end of the numerical simulation, significant portions of the initial enstrophy are still unaffected by dissipation, and the results within that time interval are minimally affected by numerical errors.

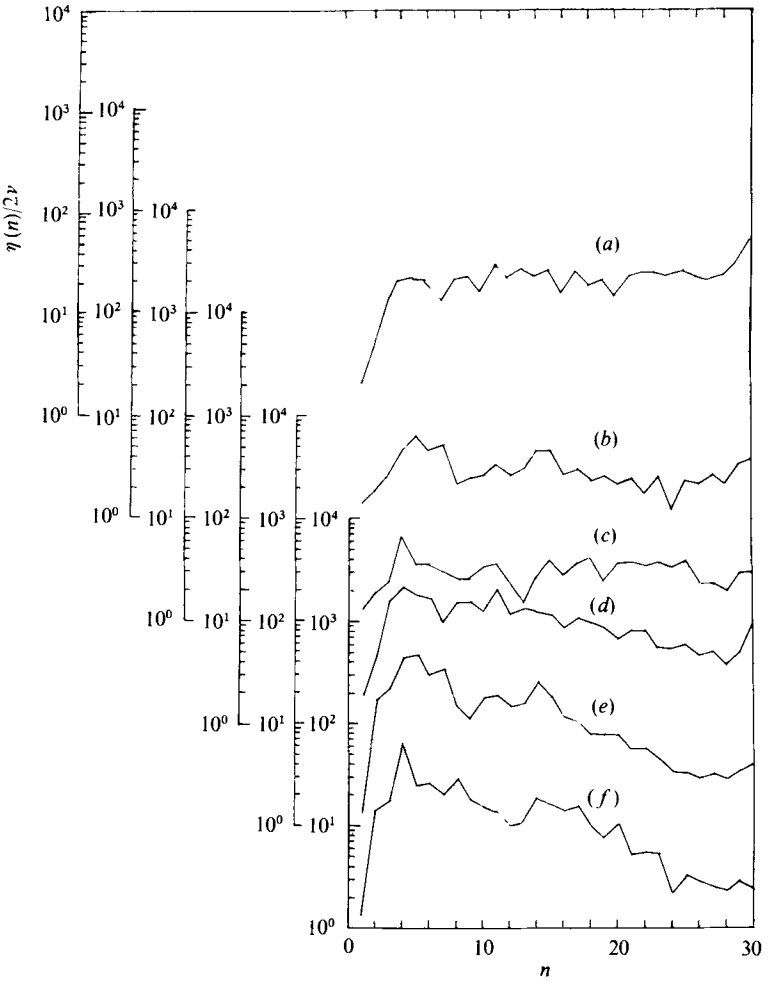

FIGURE 3. Enstrophy dissipation spectra at $t = 1{\cdot}8$. For $\nu = 0{\cdot}0025$: (*a*) Cartesian geometry; (*b*) spherical geometry without rotation; (*c*) spherical geometry with $\Omega = 1$. For $\nu = 0{\cdot}005$: (*d*) Cartesian geometry; (*e*) spherical geometry without rotation; (*f*) spherical geometry with $\Omega = 1$.

The more local transfer mechanism of spherical geometry limits the transport of enstrophy to large wavenumbers and energy to small wavenumbers. Thus the production of $\Sigma k^4 T(k)$ in Cartesian geometry is expected to be larger than that of

$$\Sigma n^2(n+1)^2 T(n)$$

in spherical geometry. The skewness factor S_2 is a non-dimensional measure of these quantities. The value of S_2 plotted in figure 5 are much larger for Cartesian than for spherical geometry.

In figure 6 we plot energy and enstrophy transfer as functions of wavenumber at $t = 1{\cdot}8$. Energy transfer to small wavenumbers is much larger in Cartesian than in spherical geometry. Enstrophy transfer in Cartesian geometry to wavenumbers larger than 15 is also larger than in spherical geometry. These observations are consistent with the differences in the transfer mechanisms.

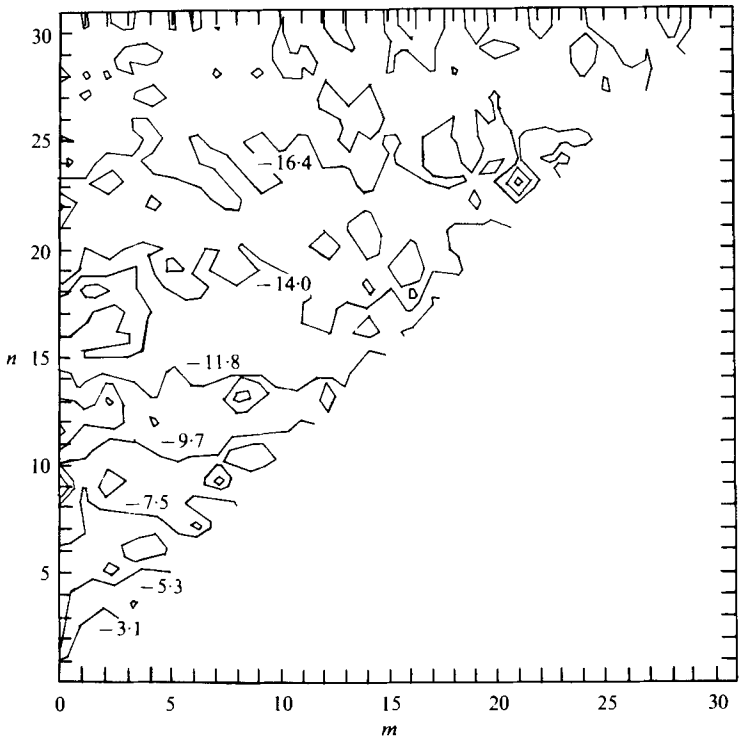

FIGURE 4. Contours of $-\ln(E(n, m))$ at $t = 2{\cdot}88$.

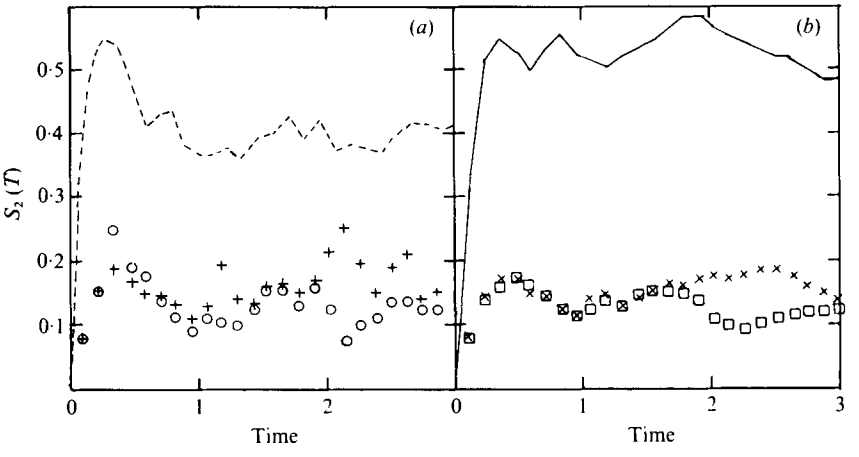

FIGURE 5. The two-dimensional skewness factor S_2. (*a*) $\nu = 0{\cdot}0025$: – – –, Cartesian geometry; ○, spherical geometry without rotation; +, spherical geometry with $\Omega = 1$. (*b*) $\nu = 0{\cdot}005$: —, Cartesian geometry; □, spherical geometry without rotation; ×, spherical geometry with $\Omega = 1$.

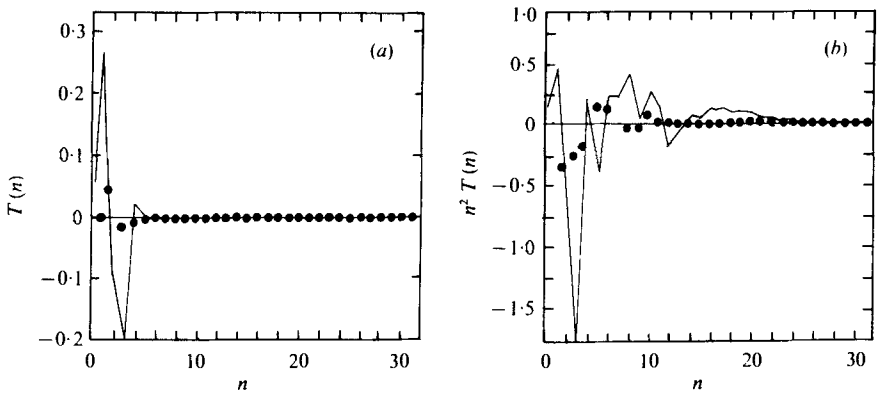

FIGURE 6. (*a*) Energy transfer and (*b*) enstrophy transfer at $t = 1{\cdot}8$. —, Cartesian geometry; ●, spherical geometry.

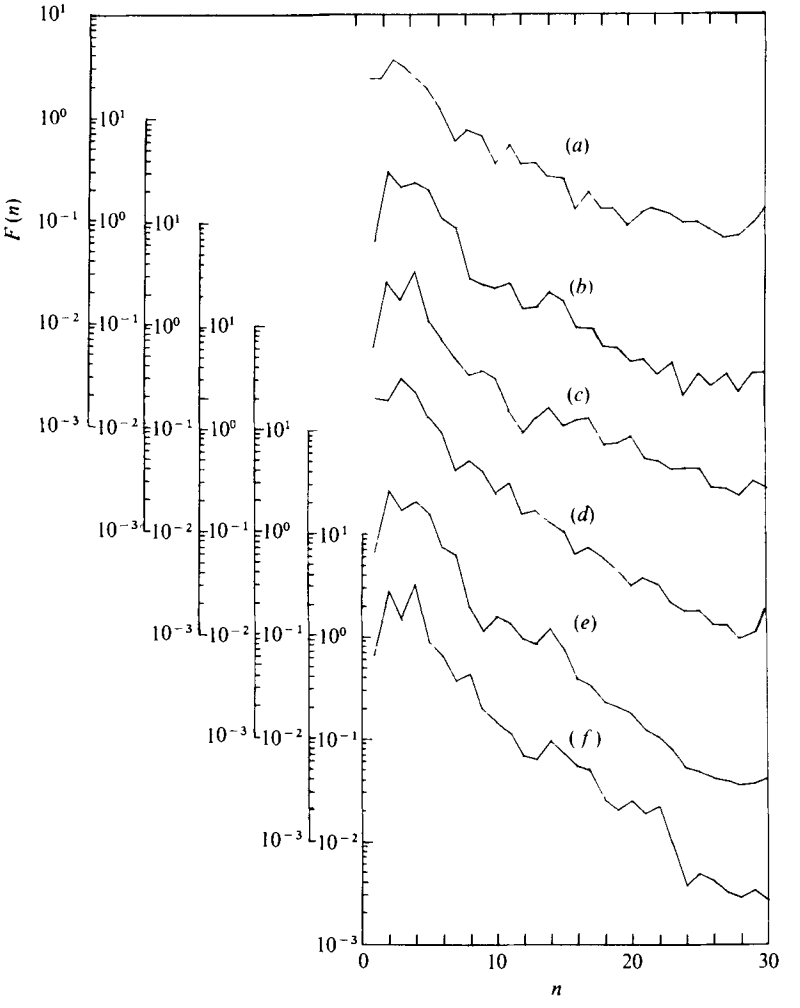

FIGURE 7. The enstrophy spectra at $t = 1{\cdot}8$. (*a*)–(*f*) as in figure 3.

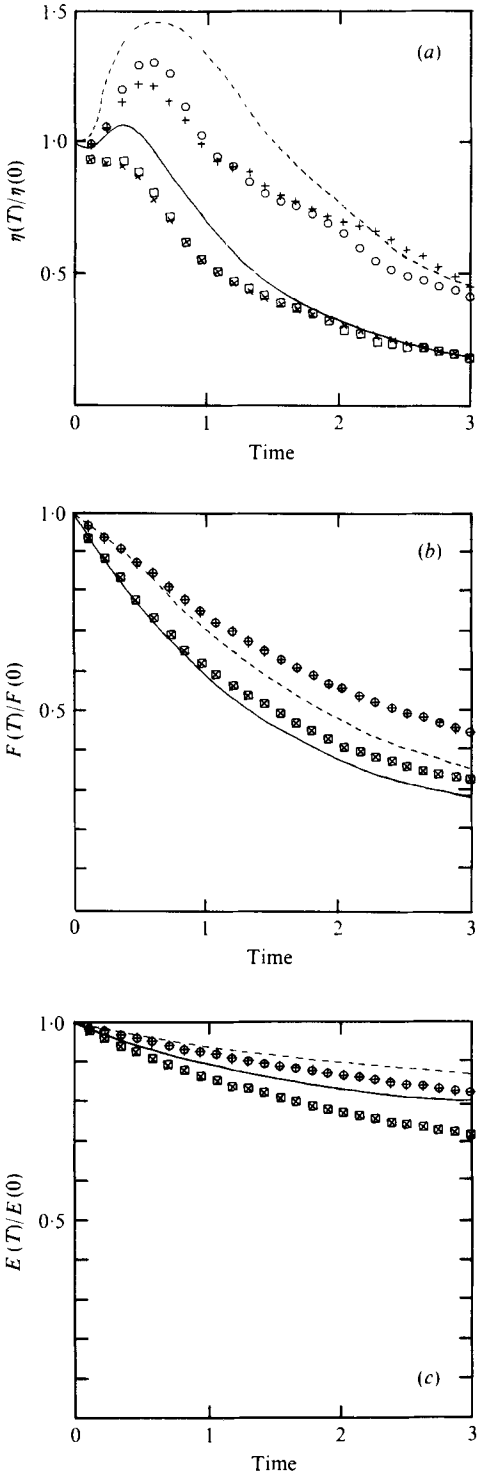

FIGURE 8. (*a*) Total enstrophy dissipation, (*b*) total enstrophy and (*c*) total energy *vs.* time. Symbols as in figure 5.

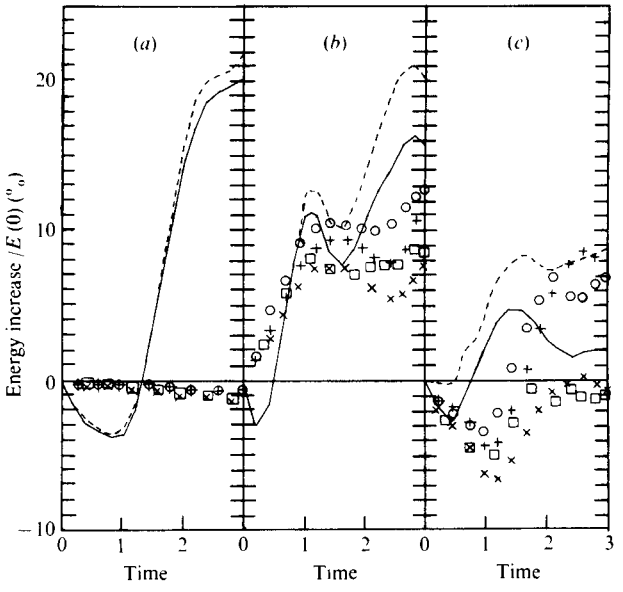

FIGURE 9. (*a*) Energy gain for $k = 1$ and $n = 1$ of Cartesian and spherical geometries respectively. (*b*) Energy gain for $k \leqslant 2$ and $n \leqslant 2$. (*c*) Energy gain for $k \leqslant 3$ and $n \leqslant 3$. Symbols as in figure 5.

Figure 7 is a plot of the enstrophy spectrum for all six tests at $t = 1{\cdot}8$. For a given Reynolds number, the enstrophies for spherical geometry with and without rotation are approximately the same, as they should be because rotation affects only large scales. With regard to enstrophy spectra, the Cartesian and spherical cases seem to agree qualitatively.

The enstrophy dissipation spectra plotted in figure 3 emphasize more strongly the effect of larger wavenumbers. Notice that the enstrophy dissipation in wavenumbers in the range 20–30 is greater compared with that in the range 3–6 in Cartesian geometry than in spherical geometry. This is consistent with the non-local transfer effect of the Cartesian geometry.

Let us now look at the total enstrophy dissipation as a function of time (see figure 8*a*). For both Reynolds numbers considered, the enstrophy dissipation is larger in Cartesian than in spherical geometry. This has already been hinted at by the enstrophy dissipation spectra.

Since the enstrophy dissipation is larger for Cartesian geometry, the enstrophies of the Cartesian cases decay faster than those for spherical geometry as shown in figure 8 (*b*). The decay rates with and without rotation in spherical geometry are almost the same.

At the same time larger amounts of energy are transferred to the small wavenumbers for non-local than for more local energy transfer. Since the smaller wavenumbers have slower decay rates, the total energy as function of time (figure 8*c*) decays more slowly in Cartesian than in spherical geometry.

The differences in the total energy levels between Cartesian and spherical geometry are much larger than the differences in the total enstrophy levels. The explanation of this result is as follows. In figure 9 we plot the energy gains relative to the total initial energy for $n \leqslant 1$, $n \leqslant 2$ and $n \leqslant 3$ (and the corresponding energy gains for $k \leqslant 1$,

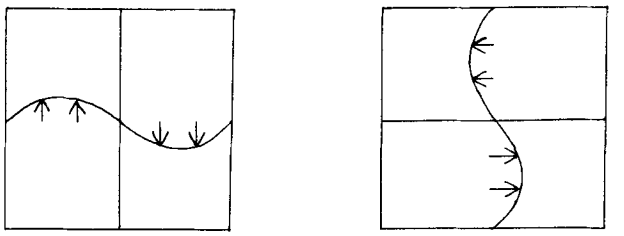

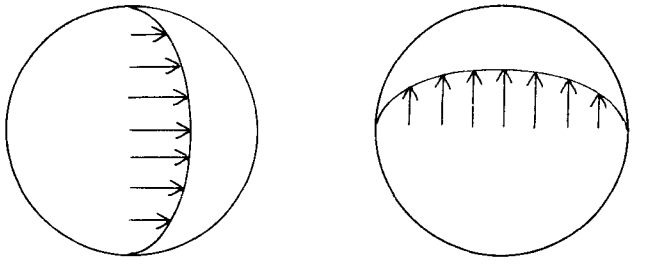

FIGURE 10. Wave structures of (*a*) $k = 1$, for Cartesian geometry, and (*b*) $n = 1$, for spherical geometry.

$k \leqslant 2$ and $k \leqslant 3$). For the cases $n \leqslant 2$ ($k \leqslant 2$) and $n \leqslant 3$ ($k \leqslant 3$), the energy gains of the spherical cases follow the general trend of the Cartesian case. The $n = 1$ mode seems to be undergoing pure decay. Conservation of momentum does not permit transfer of energy to $n = 1$ modes, because $n = 1$ modes represent uniform flow, as shown in figure 10.

Owing to the back transfer of energy, energy piles up in $k = 1$ in Cartesian geometry, while energy piles up in $n = 2$ in spherical geometry. The back transfer of energy is much larger for $k = 1$ than for $n = 2$. That is consistent with the non-local transfer mechanism for Cartesian geometry. Since Cartesian geometry contains more energy in $k = 1$ than $n = 1$, the decay rate of the total energy of Cartesian geometry is further reduced.

This work was supported by the National Science Foundation under Grant no. ATM73-06634. The computations reported here were performed at the Computing Facility of the National Center for Atmospheric Research, Boulder, Colorado, which is supported by the National Science Foundation.

REFERENCES

BAER, F. 1972 *J. Atmos. Sci.* **29**, 649.
BATCHELOR, G. K. 1969 *Phys. Fluids Suppl.* **12**, II 233.
CHARNEY, J. G. 1971 *J. Atmos. Sci.* **28**, 1087.
FJØRTOFT, R. 1953 *Tellus* **5**, 225.
HERRING, J. R., ORSZAG, S. A., KRAICHNAN, R. H. & FOX, D. G. 1974 *J. Fluid Mech.* **66**, 417.
HORN, L. H. & BRYSON, R. A. 1963 *J. Geophys. Res.* **68**, 1059.
JULIAN, P. R., WASHINGTON, W. M., HEMBREE, L. & RIDLEY, C. 1970 *J. Atmos. Sci.* **27**, 376.
KRAICHNAN, R. H. 1967 *Phys. Fluids* **10**, 1417.
LEE, T. D. 1951 *J. Appl. Phys.* **22**, 524.
LEITH, C. E. 1971 *J. Atmos. Sci.* **28**, 145.
LILLY, D. K. 1971 *J. Fluid Mech.* **45**, 395.
ONSAGER, L. 1949 *Nuovo Cimento Suppl.* **6**, 279.
ORSZAG, S. A. 1974 *Mon. Weather Rev.* **102**, 56.
TANG, C. M. 1978 Comparison of spectral methods for flows on spheres. In preparation.
WIIN-NIELSEN, A. 1967 *Tellus* **19**, 540.